Radiometer Calibration Using Colocated GPS Radio Occultation Measurements

William J. Blackwell, *Senior Member, IEEE*, Rebecca Bishop, Kerri Cahoy, *Member, IEEE*, Brian Cohen, Clayton Crail, Lidia Cucurull, Pratik Dave, Michael DiLiberto, Neal Erickson, *Member, IEEE*, Chad Fish, Shu-peng Ho, R. Vincent Leslie, Adam B. Milstein, and Idahosa A. Osaretin, *Member, IEEE*

***Abstract*—We present a new high-fidelity method of calibrating a cross-track scanning microwave radiometer using Global Positioning System (GPS) radio occultation (GPSRO) measurements. The radiometer and GPSRO receiver periodically observe the same volume of atmosphere near the Earth's limb, and these overlapping measurements are used to calibrate the radiometer. Performance analyses show that absolute calibration accuracy better than 0.25 K is achievable for temperature sounding channels in the 50–60-GHz band for a total-power radiometer using a weakly coupled noise diode for frequent calibration and proximal GPSRO measurements for infrequent (approximately daily) calibration. The method requires GPSRO penetration depth only down to the stratosphere, thus permitting the use of a relatively small GPS antenna. Furthermore, only coarse spacecraft angular knowledge (approximately one degree rms) is required for the technique, as more precise angular knowledge can be retrieved directly from the combined radiometer and GPSRO data, assuming that the radiometer angular sampling is uniform. These features make the technique particularly well suited for implementation on a low-cost CubeSat hosting both radiometer and GPSRO receiver systems on the same spacecraft. We describe a validation platform for this calibration method, the Microwave Radiometer Technology Acceleration (MiRaTA) CubeSat, currently in development for the National Aeronautics and Space Administration (NASA) Earth Science Technology Office. MiRaTA will fly a multiband radiometer and the Compact TEC/Atmosphere GPS Sensor in 2015.**

***Index Terms*—Advanced Microwave Sounding Unit (AMSU), Advanced Technology Microwave Sounder (ATMS), calibration, Compact Total Electron Count (TEC)/Atmosphere Global Positioning System (GPS) Sensor (CTAGS), CubeSat, Global Navigation Satellite System (GNSS), GPS, GPS radio occultation (RO) (GPSRO), humidity, Micro-sized Microwave Atmospheric Satellite (MicroMAS), microwave, Microwave Radiometer Technology Acceleration (MiRaTA), nanosatellite, precipitation, radiometer, remote sensing, RO, RO-Cal, temperature.**

Manuscript received May 21, 2013; revised November 8, 2013; accepted December 18, 2013. Date of publication February 13, 2014; date of current version May 22, 2014. This work was supported by the Assistant Secretary of Defense for Research and Engineering under Air Force Contract FA8721-05-C-0002.

W. J. Blackwell, C. Crail, M. DiLiberto, R. V. Leslie, A. B. Milstein, and I. A. Osaretin are with the Lincoln Laboratory, Massachusetts Institute of Technology, Lexington, MA 02420 USA (e-mail: wjb@ll.mit.edu).

R. Bishop is with The Aerospace Corporation, El Segundo, CA 90245 USA.

K. Cahoy, B. Cohen, and P. Dave are with the Department of Aeronautics and Astronautics, Massachusetts Institute of Technology, Cambridge, MA 02139 USA.

L. Cucurull is with the National Oceanic and Atmospheric Administration (NOAA) Earth System Research Laboratory, Boulder, CO 80305-3328 USA.

N. Erickson is with the University of Massachusetts, Amherst, MA 01003 USA.

C. Fish is with the Space Dynamics Laboratory, Utah State University, Logan, UT 84341 USA.

S. Ho is with the University Corporation for Atmospheric Research, Boulder, CO 80301 USA.

Color versions of one or more of the figures in this paper are available online at http://ieeexplore.ieee.org.

Digital Object Identifier 10.1109/TGRS.2013.2296558

I. Introduction

PASSIVE MICROWAVE observations from spaceborne scanning radiometers have proven profoundly useful in a variety of atmospheric applications ranging from mesoscale and synoptic numerical weather prediction to climate study [1]. Temperature sounding channels near 50–60 GHz and water vapor sounding channels near 183.31 GHz penetrate most nonprecipitating clouds and thus provide atmospheric profiling capability in almost all weather conditions. In the climate context, measurements of the atmosphere using microwave radiometry have provided a benchmark climate record of temperature trends dating back to the Microwave Sounding Unit (MSU), which began operation in 1979. MSU was followed by the Advanced Microwave Sounding Unit, which began operation in 1998. The Advanced Technology Microwave Sounder (ATMS) is the first in a series of new cross-track scanning sounders developed for the Joint Polar Satellite System. ATMS was launched on October 28, 2011 on the Suomi National Polar Partnership satellite.

The absolute calibration of spaceborne microwave scanning instruments for high-fidelity atmospheric research is immensely challenging and difficult to fully trace to a reference standard [2], although recent work has shown promise to establish brightness temperature standards with uncertainties of approximately 0.7 K [3]. As a direct result of these calibration challenges, bias corrections of up to several kelvins are routinely used [4]. Problems associated with reflector emissivity and internal calibration target (ICT) contamination have been reported [5]. Previous comparisons of Advanced Microwave Sounding Unit-A (AMSU-A) observations that were colocated to Constellation Observing System for Meteorology, Ionosphere, and Climate (COSMIC)/FORMOSAT-3 Global Positioning System (GPS) radio occultation (RO) (GPSRO) observations indicated biases as large as 1.92 K [6].

GPSRO measurements have also been used extensively to improve weather forecasting and assessments of climate [7], [8]. Temperature profile accuracies approaching 0.1 K are achievable in the upper troposphere and lower stratosphere [9], and recent work has presented techniques for probing down to the boundary layer [10]. GPSRO measurements are inherently well calibrated due to their fundamental dependence on time delays, which can be traced to the National Institute

of Standards and Technology (NIST) standards [6]. However, GPSRO measurements have relatively sparse geospatial coverage. When the COSMIC/FORMOSAT-3 constellation was at peak operational capacity, it provided approximately 2000 occultation profiles per day, compared with over 3 000 000 soundings per day for ATMS.

In this paper, we explore the combined use of passive microwave sounding and GPSRO observations to leverage the benefits of both in order to achieve highly accurate calibration with dense geospatial sampling. Furthermore, we investigate a new method of two-point calibration, where the traditional calibration points of cold sky and warm ICT are replaced with cold sky and a warm noise diode turned on and off against cold sky. The noise from the diode is sufficiently strong that a weak coupler can be used to avoid the need for a switch—the noise diode is always in the signal path but only produces noise when energized with an appropriate bias current (usually on the order of 5–10 mA). The noise diode is periodically calibrated with GPSRO measurements to mitigate any drift [11]. In addition to offering improved calibration, this method also dispenses with the need for an ICT, which can be bulky and susceptible to errors and often drives the design of the radiometer antenna and scanning system. GPSRO instrumentation, however, is very compact and places no restrictions on the design of the radiometer. In fact, the "CubeSat" class spacecraft ($10 \times 10 \times 30$ cm; 4.0 kg) can now accommodate radiometers [12] and GPSRO systems [13] on the same spacecraft, offering a low-cost high-performance sounding platform.

This paper is organized as follows. First, we provide an overview of the calibration technique (henceforth "RO-Cal") and describe how it could be implemented on a 50–60-GHz (V-band) radiometer system. We then describe the method in a detailed step-by-step manner, simulate its performance using the NOAA88b global profile set, and examine the effect of the minimum GPSRO sounding altitude (which drives the required SNR and GPSRO antenna gain requirements) on calibration performance. We then present an end-to-end RO-Cal radiometer calibration simulation. Finally, we describe the Microwave Radiometer Technology Acceleration (MiRaTA) CubeSat that will be used to validate the technique with a launch in 2015.

II. Overview of the RO-Cal Methodology

The RO-Cal calibration method involves two core operations to synergistically use GPSRO and microwave radiometer measurements for the observing geometry shown in Fig. 1. First, a quadratic relationship between the GPSRO refractivity profile versus tangent height, $N(h)$, and radiometer brightness temperatures at a particular observing angle and frequency band of interest, $T_B(\theta, f)$, is derived. Second, the radiometer gain g (kelvin/count, where "count" is the output of a 16-b A/D converter) is chosen to minimize the residual between the calibrated and the GPSRO-derived brightness temperature. Errors due to the quadratic estimation are treated in a weighted least squares sense. In this paper, we consider two cases, one where the angular coincidence between the refractivity profile and the radiometer observations is perfect, for which a closed-form expression for g can be derived, and one where there is

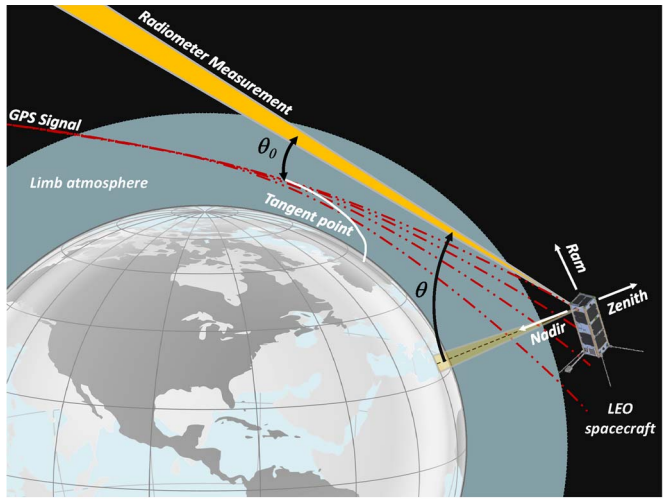

Fig. 1. Basic geometry of the GPSRO microwave radiometer calibration problem is shown, including some distortions to emphasize key features, such as the radiometer scan angle θ, GPSRO tangent points, and radiometer pointing error in the scan plane $\widehat{\theta_0}$.

an unknown scalar angular offset θ_0 between the refractivity profile and the radiometer observations, thus requiring a numerical minimization routine to solve for both g and θ_0. Note that, in practice, the error θ_0 could arise from a number of factors, including errors in the spacecraft attitude determination system, imperfect knowledge of the electrical boresight of the antenna pattern, and errors in the mechanical mounting of the radiometer to the spacecraft. A block diagram summarizing the method components is shown in Fig. 2.

A. Description of the Profile Data and Models Used to Evaluate the RO-Cal Performance

The performance analyses in this paper are all based on simulated observations derived using physical models and global ensembles of atmospheric states. These include the NOAA88b atmospheric profile data set and surface emissivity values, a microwave/millimeter wave nonscattering radiative transfer model, and the use of the NOAA88b temperature profiles to generate simulated GPSRO refractivity profiles. The selection of the ensemble of atmospheric states is a critically important part of any simulation study, and we have taken great care to ensure that the profiles included in the analysis are sufficiently representative of a variety of atmospheres that challenge most atmospheric sounding systems.

1) NOAA88b Atmospheric Profile Data Set: The NOAA88b radiosonde/rocketsonde data set contains global profiles that are distributed seasonally and geographically. For this study, 1000 profiles were randomly chosen from the 7547 available profiles to allow all of the spectral and spatial convolution operations performed on the data to be executed in several days. Atmospheric temperature, moisture, and ozone are given at 100 discrete levels from the surface to altitudes exceeding 50 km. Skin surface temperature is also recorded. Additional details on the geographic representation of the profiles and the profile variability can be found in [14].

2) Microwave Surface Emissivity: Surface emissivity values from the NOAA88b data set were used. These include

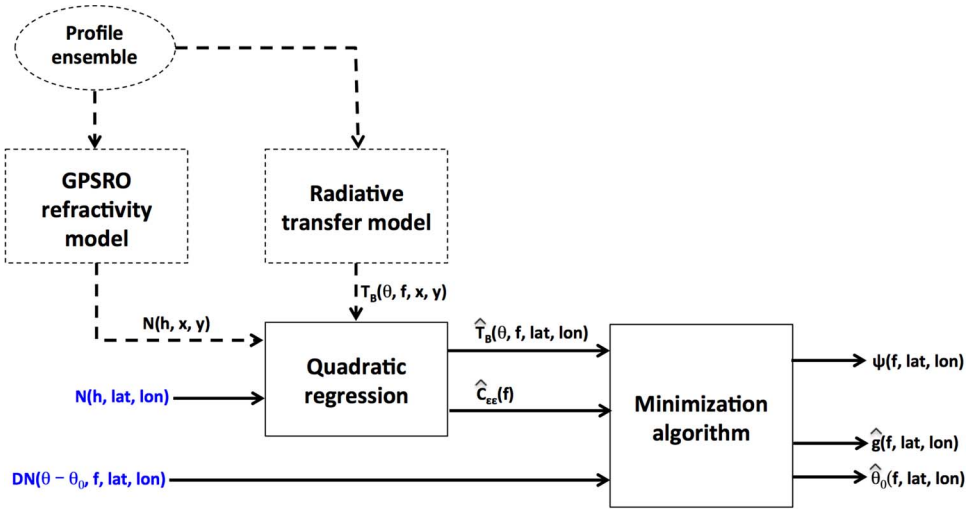

Fig. 2. Block diagram of the GPSRO microwave radiometer calibration procedure. Dashed lines indicate operators that are trained offline using ensemble data sets (NOAA88b in this case). The inputs to the algorithm are radiometer counts (DNs) and the refractivity profile $N(h)$. Outputs are the estimated radiometer gain g and the estimated angular error in the radiometer scan plane $\widehat{\theta_0}$.

land and ocean emissivities and range from 0.5 to 0.6 over ocean and from 0.7 to 0.98 over land. We note that surface emissivity is a relatively weak contributor to brightness temperature for the frequencies and viewing angles considered in this study (a key feature of the method, because interference due to surface emissivity uncertainty is minimized).

3) Microwave/Millimeter-Wave Nonscattering Radiative Transfer Models: Simulated brightness temperature observations for atmospheric profiles in the NOAA88b data set were calculated using the TBARRAY software package of Rosenkranz [15], which was modified to introduce spherical symmetry and accommodate radiative transfer calculations through the Earth's limb. TBARRAY is a line-by-line routine based on the Liebe millimeter-wave propagation model [16], [17]. Scattering was not modeled because cloud liquid water content is not recorded in the NOAA88b data set. This is not a consideration in this work because scattering effects can be flagged by the calibration algorithm (see Section IV-B). The spectral passbands were modeled as boxcar functions using approximately ten discrete frequencies per passband.

4) GPSRO: GPSRO receivers on low Earth orbiting (LEO) satellites receive radio-frequency signals from higher altitude GPS satellites. As the LEO satellite and its GPSRO receiver drop behind the Earth's limb from the perspective of the GPS satellite (an ingress occultation), the signal penetrates through the atmosphere from space down to the surface; rising occultations are also used. The path of the signal is affected as it passes through the refractivity gradient of the atmosphere and results in a measurable frequency deviation in the received signal. The GPS radio-frequency signals are traceable to NIST standards (the SI second) with a high degree of accuracy using monitoring and corrections from a series of atomic clocks. The frequency measurement and knowledge of the geometry, in addition to assumptions of spherical symmetry, yield a profile of refractivity as a function of altitude (geometric height) $N(h)$, from which temperature and pressure can be derived when water vapor is negligible [6], [9], [18]–[20].

Refractivity (N) is defined in terms of refractive index n as

$$N = (n - 1) \cdot 10^6. \tag{1}$$

In the Earth's neutral atmosphere, refractivity is approximately related to the pressure (P), the temperature (T), and the partial pressure of water vapor (P_W) by the following equation [21]:

$$N = 77.6\frac{P}{T} + 3.73 \times 10^5 \frac{P_W}{T^2}. \tag{2}$$

We note that a more accurate relationship is given in [22], but the simple relationship above is used here. In this paper, the NOAA88b temperature and water vapor profiles, defined at fixed pressure levels, are used with (2) to generate refractivity as a function of pressure. Note that, at lower altitudes in moist tropical regions, the estimated GPSRO refractivity may significantly depend on the moisture distribution. In the upper troposphere and stratosphere where moisture is negligible, the refractivity noise in the fractional refractivity can be as small as 0.2% (see [9, Fig. 13]). Currently, multiyear GPSRO data can be obtained from six different RO centers (see [20] for details). By using the differences and standard deviations of the individual centers relative to the intercenter mean to quantify the structural uncertainty, it was confirmed that the mean refractivity anomalies among centers agree within 0.01% with a standard deviation of 0.2% (see [20, Table 2]). In this paper, we add a random refractivity noise commensurate with that reported by Kursinski *et al.* [9] in the calculated refractivity.

III. Estimation of Radiometer Brightness Temperature From GPSRO Refractivity

The first step of the calibration algorithm involves a quadratic regression on the GPSRO refractivity profile, $N(h)$, to estimate the radiometer brightness temperature as a function of the scan angle through the Earth's limb, $T_B(\theta, f)$. It is assumed that the radiometer is sampled such that there is a uniform 0.1-degree spacing between the limb observations.

TABLE I
SPECTRAL CHARACTERISTICS OF THE RADIOMETER CHANNELS CONSIDERED IN THIS STUDY

Channel #	Center Frequency (GHz)	Bandwidth (MHz)
1	52.85	600
2	53.50	600
3	54.15	600
4	54.75	600
5	55.35	600
6	56.00	600
7	183.31 ± 1	500
8	183.31 ± 3	1000
9	183.31 ± 7	2000
10	207.4	2000

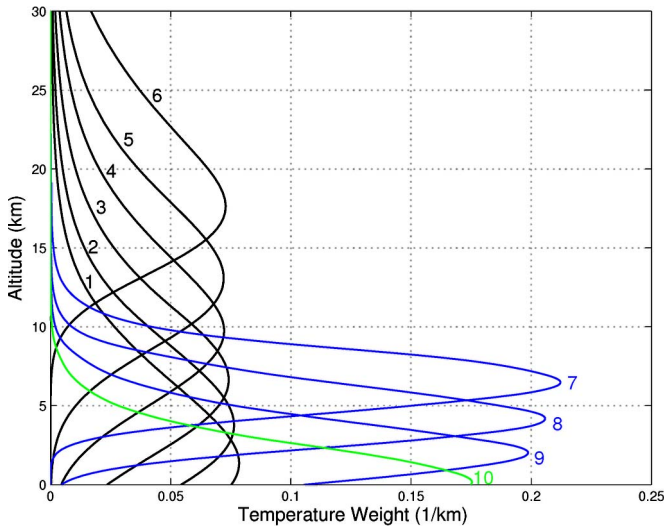

Fig. 3. Weighting functions for the channels considered in this study at nadir incidence over a nonreflective surface. The U.S. 1976 standard atmosphere was used for the calculations.

A. Radiometer Assumptions

For the simulations in this paper, we consider six channels in the 50–60-GHz temperature sounding band (also denoted "V-band"), three channels in the 183.31-GHz water vapor sounding band, and one channel at 206.4–208.4 for cloud ice sensing. The latter four channels are also denoted "G-band." Channel passbands are given in Table I, and weighting functions for the temperature channels are shown in Fig. 3. These channels closely approximate similar channels on ATMS, with the exception of the 207.4-GHz channel, which is added for consideration in this study. A spacecraft altitude of 400 km is assumed, corresponding closely to the expected initial orbit altitude of MiRaTA (see Section V). The antenna beamwidth is 5.0° [full-width at half-maximum (FWHM)] at 50 GHz and 1.25° FWHM at 200 GHz. Gaussian beam shapes are assumed in the spatial convolution operators. A receiver temperature of 300 K was assumed for the V-band channels; 1000 K was assumed for the G-band channels. A scan rate of one revolution per second was assumed. At 0.1-degree angular spacing, the integration time for each observation is therefore approximately 275 μs. A 20-point triangular filter was used to reduce the sensor noise in the calibration, as similar filters have been used operationally with ATMS. With these assumptions, typical radiometer sensitivity [rms noise-equivalent delta temperature (NEDT)] values range from 0.2 K (3 K scene) to 0.3 K (250 K scene) for the V-band channels and range from 0.35 K (5 K scene and 2000-MHz bandwidth) to 0.85 K (250 K scene and 500-MHz bandwidth) for the G-band channels, where we note that the NEDT increases with increasing scene temperature but decreases with increasing channel bandwidth.

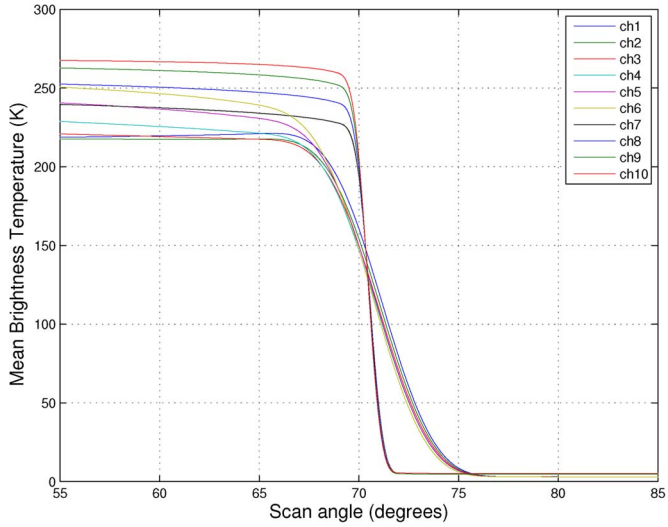

Fig. 4. Mean brightness temperatures calculated for the NOAA88b data set are shown for each of the ten channels considered in this study (see Table I). The V-band (with 5.0-degree FWHM antenna beamwidth) and G-band channels (with 1.25-degree FWHM antenna beamwidth) are shown. The G-band brightness temperature curves are characterized by a steeper slope due to their narrower antenna beamwidth.

The mean brightness temperatures for the NOAA88b set plotted as a function of sensor scan angle are shown in Fig. 4 for the viewing geometry assumptions described earlier. The "limb" portion of the Earth's atmosphere occurs over a range of angles centered at approximately 71°. It should be noted that the Rayleigh–Jeans approximation cannot be used for temperatures below approximately 150 K, and spectral radiance intensities must be evaluated directly using the Planck function.

B. Results

Brightness temperature retrieval performance results for the V-band temperature channels as a function of scene temperature are shown in Fig. 5, and results for the G-band channels are shown in Fig. 6, where the entire brightness temperature distribution shown in Fig. 4 is included in these figures. The sensitivity to GPSRO penetration depth is also shown—the less transparent (more opaque) channels are relatively insensitive to penetration depth, while the more transparent (less opaque) channels are highly sensitive to penetration depth. Retrieval errors of 0.5 K or less are evident for the more opaque V-band channels and degrade by several degrees for the less opaque V-band channels. Errors for the G-band channels range from approximately 1 K to 4 K.

The retrieval error $\epsilon(\theta, f) = T_B(\theta, f) - \widehat{T}_B(\theta, f)$ for each channel is characterized by an error covariance matrix, $\mathbf{C}_{\boldsymbol{\epsilon\epsilon}}(f)$, where each row and column is associated with a single radiometer view angle. This error covariance will be used in the subsequent minimization routine to estimate the radiometer gain g.

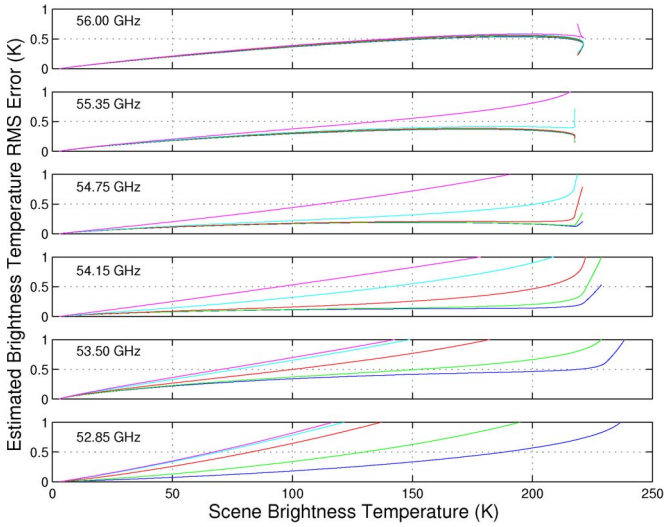

Fig. 5. RMS error for the retrieval of V-band brightness temperature from GPSRO refractivity profiles. Each set of five lines indicates GPSRO penetration depths of 8, 10, 12, 16, and 20 km, with 8 km yielding the lowest errors and 20 km yielding the highest errors in all cases.

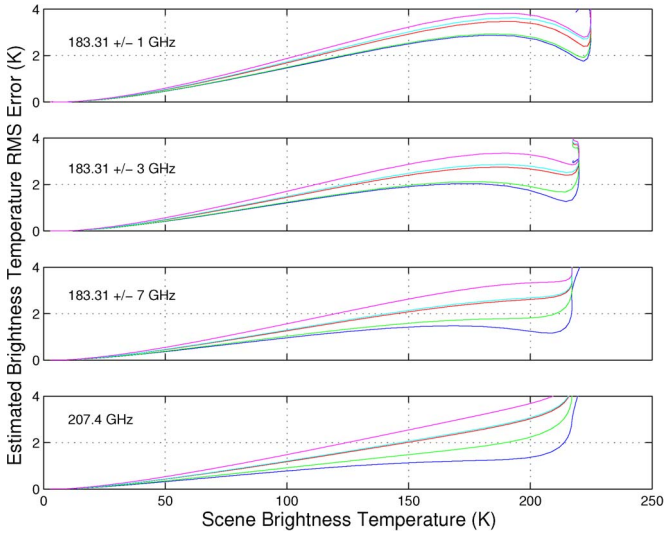

Fig. 6. RMS error for the retrieval of G-band brightness temperature from GPSRO refractivity profiles. Each set of five lines indicates GPSRO penetration depths of 8, 10, 12, 16, and 20 km, with 8 km yielding the lowest errors and 20 km yielding the highest errors in all cases.

IV. Estimation of Radiometer Gain

The second component of the RO-Cal algorithm uses the retrieved brightness temperatures $\widehat{T}_B(\theta, f)$ as a temperature reference from which radiometer gain g is derived. If there is no angular offset between the retrieved and actual brightness temperatures, a closed-form solution can be derived for g using weighted least squares. The cost function to be minimized (for each channel) is

$$\Psi = (\widehat{\mathbf{T}}_\mathbf{B} - \widetilde{\mathbf{T}}_\mathbf{B})' \mathbf{C}_{\boldsymbol{\epsilon\epsilon}}^{-1} (\widehat{\mathbf{T}}_\mathbf{B} - \widetilde{\mathbf{T}}_\mathbf{B}). \tag{3}$$

We have used the boldface type to indicate that angular dependence has been captured as elements in vectors or matrices, and $\widetilde{\mathbf{T}}_\mathbf{B}$ is the calibrated radiometer brightness temperature defined as follows:

$$\widetilde{\mathbf{T}}_\mathbf{B} = g(\mathbf{DN} - DN_c) + T_c \tag{4}$$

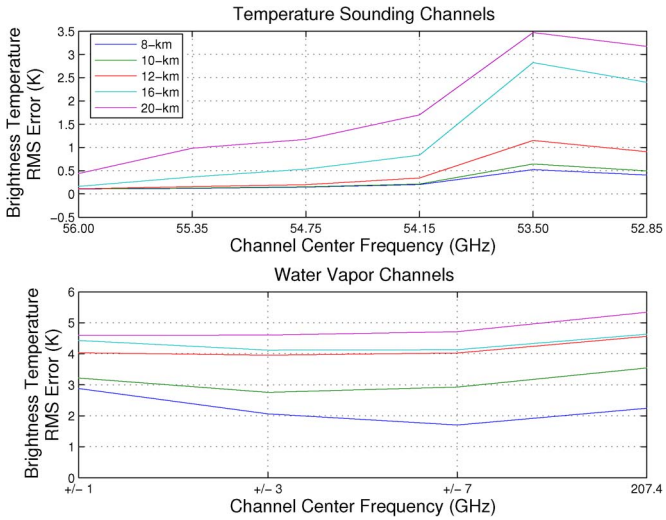

Fig. 7. RMS error for calibrated brightness temperature for a 300 K scene assuming perfect angle knowledge. The G-band channel center frequencies in the lower panel are 183.31 ± 1, 183.31 ± 3, 183.31 ± 7, and 206.4–208.4 GHz.

where DN is the radiometer count output (digital number) when viewing the limb, DN_c is the radiometer output when viewing cold sky, and T_c is the cold sky brightness temperature.

For the simulations presented hereinafter, the radiometer gain (kelvin/count) for each profile was assigned a Gaussian random value with a mean of 0.02 and a standard deviation of 0.0012, which is representative of radiometer behavior at the frequencies of interest in this study. For cases with a nonzero angular offset θ_0 between $\widehat{\mathbf{T}}_\mathbf{B}$ and $\widetilde{\mathbf{T}}_\mathbf{B}$, a Gaussian random value was assigned to θ_0 with a mean of zero and a standard deviation of one, which is representative of current commercially available CubeSat attitude and determination systems. Approximately 200 scan angles ranging from 55° to 75° were used for the V-band calibrations, and approximately 40 scan angles ranging from 67° to 71° were used for the G-band calibrations.

A. Case I: No Angular Offset

If there is no angular offset between $\widehat{\mathbf{T}}_\mathbf{B}$ and $\widetilde{\mathbf{T}}_\mathbf{B}$, then $\widehat{g}$ can be expressed in closed form as

$$\widehat{g} = \frac{(\widehat{\mathbf{T}}_\mathbf{B} - T_c)' \mathbf{C}_{\boldsymbol{\epsilon\epsilon}}^{-1} (\mathbf{DN} - DN_c)}{(\mathbf{DN} - DN_c)' \mathbf{C}_{\boldsymbol{\epsilon\epsilon}}^{-1} (\mathbf{DN} - DN_c)}. \tag{5}$$

The rms calibration errors for this case are shown in Fig. 7 when calibrating a 300 K scene. The V-band performance is excellent (approximately 100 mK) for opaque channels with GPSRO penetration depths down to 12 km, and performance degrades with decreasing penetration depth, markedly so for nonopaque channels. G-band calibration performance is not as good, with errors of several kelvins.

B. Case II: Constant Angular Offset

We now examine a case with an unknown but constant angular offset θ_0 between $\widehat{\mathbf{T}}_\mathbf{B}$ and $\widetilde{\mathbf{T}}_\mathbf{B}$. Now, a more sophisticated method is needed to minimize (3) because the radiometer gain and offset angle must be jointly optimized. We define a

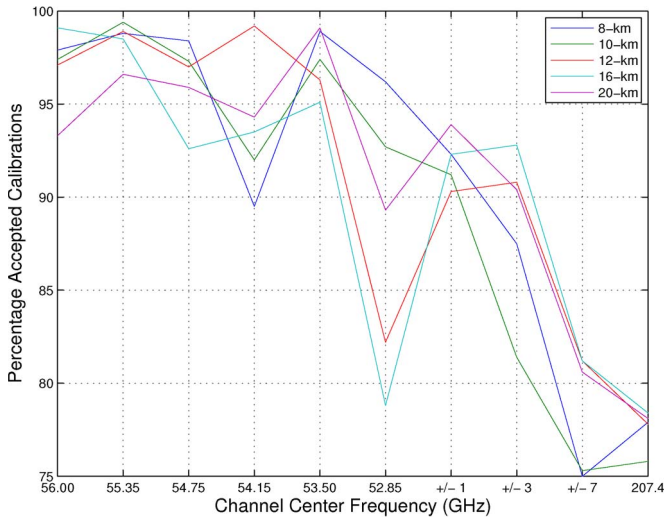

Fig. 8. Percentage of successful calibrations for each of the ten channels.

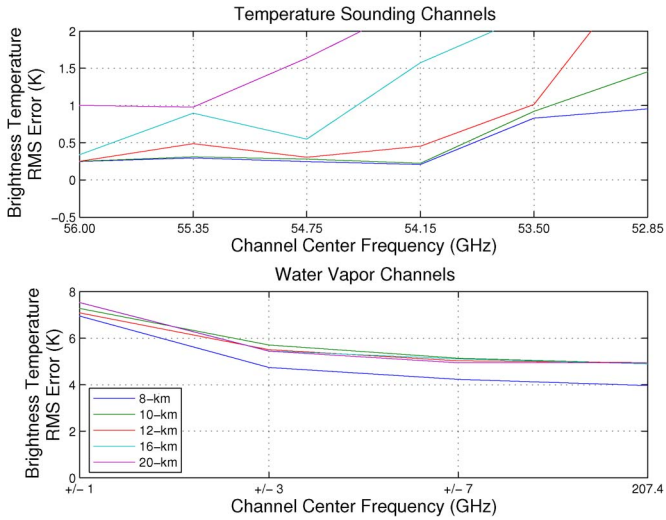

Fig. 9. RMS error for calibrated brightness temperature for a 300 K scene with angle offset retrieved from observations. The G-band channel center frequencies in the lower panel are 183.31 ± 1, 183.31 ± 3, 183.31 ± 7, and 206.4–208.4 GHz.

"shifted" $\widetilde{\mathbf{T}}_{\mathbf{B}}$, $\widetilde{\mathbf{T}}_{\mathbf{B}}^{\mathbf{S}}$, such that $\widetilde{\mathbf{T}}_{\mathbf{B}}^{\mathbf{S}} = \widetilde{\mathbf{T}}_{\mathbf{B}}(\theta - \theta_0)$, and a new cost function is minimized

$$\Psi = \left(\widehat{\mathbf{T}}_{\mathbf{B}} - \widetilde{\mathbf{T}}_{\mathbf{B}}^{\mathbf{S}}\right)' \mathbf{C}_{\epsilon\epsilon}^{-1} \left(\widehat{\mathbf{T}}_{\mathbf{B}} - \widetilde{\mathbf{T}}_{\mathbf{B}}^{\mathbf{S}}\right). \tag{6}$$

The Nelder–Mead simplex method [23] was used to numerically minimize (6), given $\widehat{\mathbf{T}}_{\mathbf{B}}$ and initial guesses for radiometer gain and offset angle. The parameter mean values were used for the initial guesses, as frequent noise diode calibrations should produce $\widehat{g}$ estimates within a fraction of a percent of the true values [11].

A very useful diagnostic is the value of the cost function (6) after minimization, as this can be used for the quality control of the estimated values. We declare a "failure to converge" condition if the cost function exceeds 200 (the number of angles used) for the V-band channels and 40 (the number of angles used) for the G-band channels. The percentage of successful calibrations is shown in Fig. 8. Opaque channels are almost always successfully calibrated, although the success rate drops to approximately 75% for the G-band channels.

The rms calibration errors for this case are shown in Fig. 9 when calibrating a 300 K scene. V-band performance is still very good, degrading to approximately 0.25 K for the opaque channels for GPS penetration depths down to 12 km, and performance degrades with decreasing penetration depth, markedly so for nonopaque channels. G-band calibration performance is not as good, with errors exceeding 4 K.

The locations of the rejected calibrations were examined for evidence of any geographically problematic regions. The locations of all 1000 profiles and the rejected calibrations for the 207.4-GHz channel with a 20-km GPSRO penetration depth (the worst performing case) are shown in Fig. 10. The locations of rejected cases are uniformly distributed around the globe with no obvious geographical correlations.

The angular offsets were also retrieved as part of the calibration process. The angle retrieval rms error is shown in Fig. 11. The results are quite good, as accuracies better than 0.005° (approximately 85 microradians or 18 arcseconds) are achieved for opaque channels. This level of pointing knowledge (in the sensor scan plane) is commensurate with that achievable with star tracking systems.

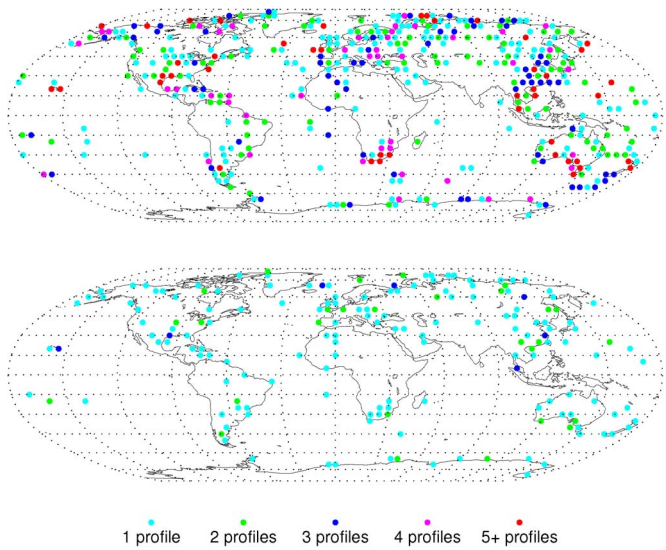

Fig. 10. Locations of all 1000 profiles used in this study are shown in the top panel, and the locations of the rejected calibrations for the 207.4-GHz channel with a 20-km GPSRO penetration depth (worst case) are shown in the bottom panel.

C. Discussion

These results are very encouraging, considering that the 0.25 K rms calibration error shown in Fig. 9 is one-third of the desired calibration error of the state-of-the-art ATMS [24] launched in 2011. The trend of decreasing calibration error with increasing V-band channel opacity evident in Figs. 7 and 9 suggests that further performance improvements could be gained by the addition of more opaque channels. For example, a channel centered near 58.4 GHz with similar bandwidths to those considered in this study would peak near 25 km. If noise

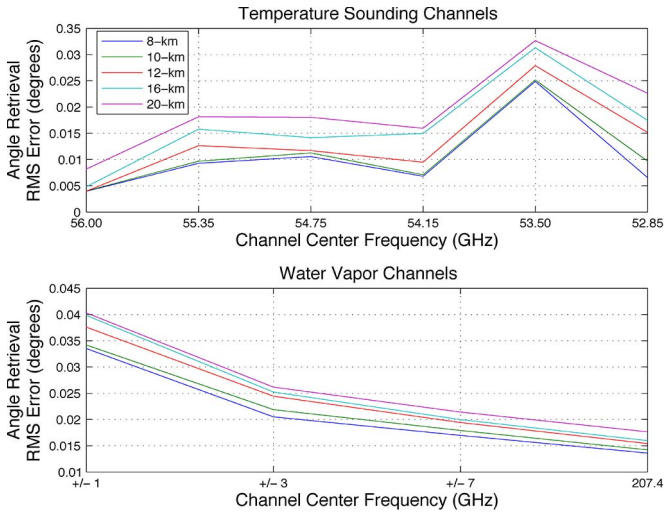

Fig. 11. RMS error for angle offsets retrieved from observations using the RO-Cal algorithm.

diode drift is highly correlated within the frequency passband of the diode, only a single calibration point using an opaque channel would be needed, thereby permitting GPSRO penetration depths down only to the stratosphere. This could be accomplished with a relatively small GPSRO antenna compatible with CubeSat implementation. We note that the G-band channels are not easily calibrated with this technique due primarily to water vapor variability to which the GPSRO measurements are largely blind. Possible enhancements that might improve performance include more sophisticated estimators for $\widehat{\mathbf{T}}_{\mathbf{B}}$, inclusion of additional atmospheric data from radiosondes or numerical weather prediction fields, inclusion of channels with more opacity, and treatment of channels simultaneously instead of individually. We also suggest the consideration of RO with frequencies capable of measuring water vapor.

V. Future Validation of the Methodology With the MiRaTA Spacecraft

The RO-Cal methodology is particularly appealing for nanosatellite sounders, which typically have relatively simple attitude determination systems capable of pointing knowledge on the order of a degree and are severely volume and mass constrained, precluding the use of blackbody ICTs. In this section, we briefly describe how the RO-Cal technique will be validated as part of the MiRaTA CubeSat mission scheduled for launch in 2015 into an orbit with a 390-km initial altitude and a 52-degree inclination. The MiRaTA CubeSat will carry out the mission objectives over a 90-day mission, including the on-orbit checkout and validation period. MiRaTA is a 3U (30 cm $\times$ 10 cm $\times$ 10 cm) CubeSat comprising V- and G-band radiometers (52–58 GHz, 175–191 GHz, and 206.4–208.4 GHz) developed by MIT Lincoln Laboratory and the University of Massachusetts at Amherst, the Compact TEC/Atmosphere GPS Sensor (CTAGS) with five-element patch antenna array developed by The Aerospace Corporation, and CubeSat spacecraft subsystems for attitude determination and control, communications, power, and thermal control to be integrated by the MIT Space Systems Laboratory. Ground segment and mission operations will be coordinated by the NASA Wallops Flight Facility and the Space Dynamics Laboratory. The spacecraft dimensions are $10 \times 10 \times 34$ cm, the total mass is 4.0 kg, and the total average power consumption is 6 W.

A. ConOps

The primary MiRaTA mission concept of operations (ConOps) is summarized in Fig. 12. The MiRaTA spacecraft will perform a slow pitch up/down maneuver once per orbit to permit the radiometer and GPSRO observations to sound overlapping volumes of atmosphere through the Earth's limb, where sensitivity, calibration, and dynamic range are optimal. These observations will be compared to radiosondes, to global high-resolution analysis fields, to other satellite observations (for example, ATMS and the Cross-track Infrared Sounder on the Suomi National Polar Partnership (NPP) satellite), and with each other (GPSRO and radiometer) using radiative transfer models.

B. Spacecraft Overview

The MiRaTA spacecraft is shown in Fig. 13. There are no moving mechanisms, and the only deployable structures (both with flight heritage) are two solar panels and a simple tape-spring antenna for UHF communications with the NASA Wallops Flight Facility 18.3-m ground station. The radiometers view the Earth through the nadir deck of the spacecraft, and in this frame, the GPSRO patch antennas have a field of view in the zenith direction, which is oriented to the limb during GPSRO sounding via a simple pitch or roll maneuver (see Fig. 12). A separate GPS antenna is used for precision orbit determination during the maneuver. The radiometer and GPSRO fields of view are used to probe the same volume of atmosphere by using the control authority of the reaction wheel assembly to rotate the spacecraft about either the pitch or roll axes approximately once per orbit.

The MiRaTA CubeSat will contain two complete instrument systems, a triband atmospheric sounder and CTAGS, which is based on work described in [13]. These two instruments will be operated in a manner to allow cross-comparison and cross-calibration. The triband microwave atmospheric sounder provides colocated observations over three frequency bands, 52–58 GHz, 175–191 GHz, and 206.4–208.4 GHz, and comprises two radiometer subsystems: 1) the V-band (52–58 GHz) front-end receiver with a weakly coupled noise diode, a low-noise Monolithic Microwave Integrated Circuit (MMIC) amplifier, a mixer, an intermediate frequency (IF) preamplifier, and an ultracompact IF spectrometer with highly scalable Low-Temperature Co-fired Ceramic (LTCC)/Substrate Integrated Waveguide (SIW) architecture operating over the 23–29-GHz IF band to provide six channels with temperature weighting functions approximately uniformly distributed over the troposphere and lower stratosphere (see Fig. 3) and 2) the broad-band G-band mixer front end operating from 175.31 to 208.4 GHz with a conventional IF spectrometer with lumped element filters. Approximately 1000 GPSRO + radiometer Earth limb scans are expected over the course of the mission.

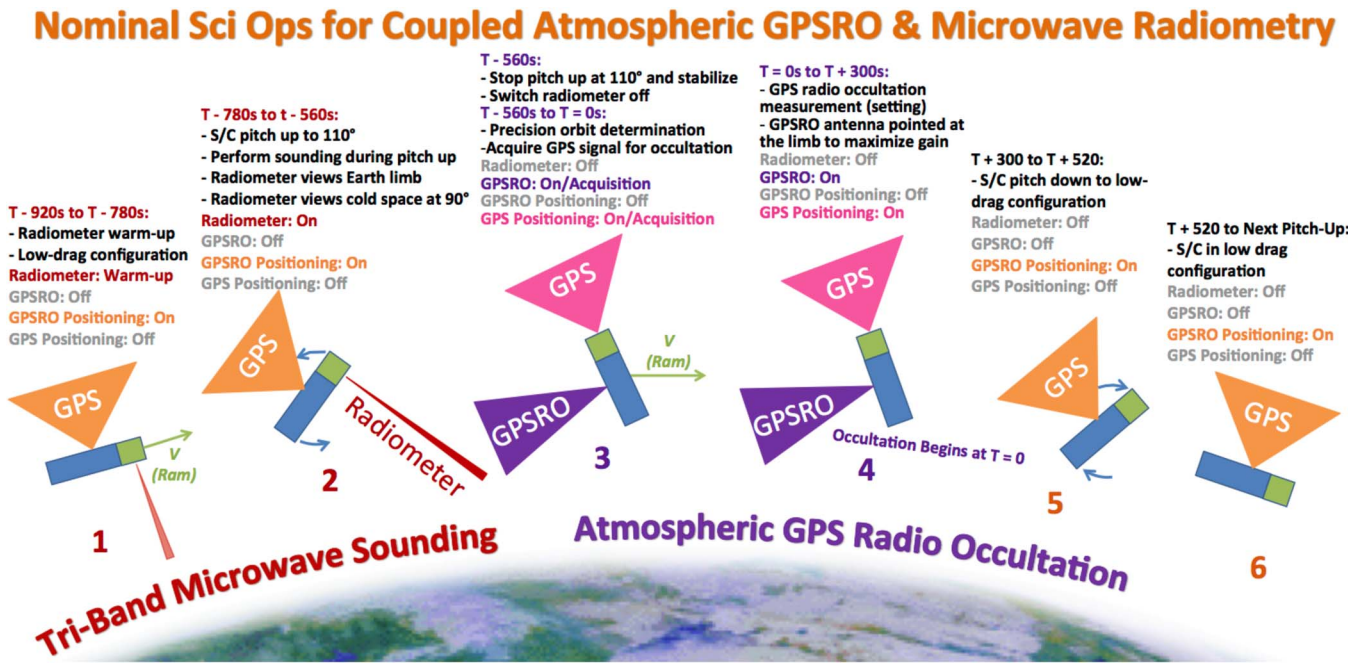

Fig. 12. MiRaTA primary mission validation ConOps is shown. A slow pitch maneuver (0.5°/s) is used to scan the radiometer field of view through the Earth's limb and subsequently direct the GPSRO field of view through the same atmosphere to catch a setting occultation. The entire maneuver takes about 20 min.

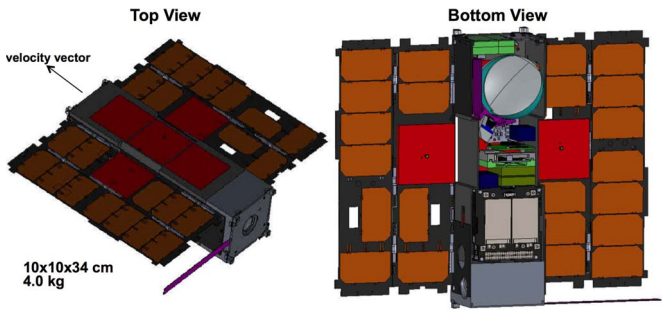

Fig. 13. View looking down onto the top of the MiRaTA spacecraft is shown on the left, and a view of the bottom of the spacecraft (with the bottom body panel removed for illustration) is shown on the right. The five-element antenna patch array on the zenith deck of the spacecraft is used for the atmospheric GPSRO measurements. The side patches are integrated onto deployable solar panels (mounted beneath the substrate) for simplicity and reliability. The primary spacecraft components are visible in the image on the right, including the following (from the bottom up): three-axis reaction wheel assembly, avionics and power stack (batteries visible), GPS receivers (two), and radiometer components. The side patch antennas fold inward and occupy a fraction of space along the body panels of the spacecraft prior to deployment. The holes in the deployed solar panels allow access to spacecraft electronics. A representative UHF tape-spring antenna is shown for illustration purposes—the flight version will likely be positioned on the lower deck of the spacecraft to permit the use of a larger ground plane.

VI. Summary and Future Work

We have presented a new radiometer calibration method that uses frequent observations of noise diodes and infrequent GPSRO measurements to calibrate any drift in the noise diode output. This method offers improved accuracy relative to traditional methods while being easier to accommodate on very small spacecraft with coarse attitude determination capabilities. Simulation analyses indicate that absolute accuracies approaching 0.25 K are obtainable for opaque V-band channels. If diode drift is highly correlated with frequency, this calibration can be readily transferred to nonopaque channels. The MiRaTA CubeSat mission is in development to validate the simulation results presented here, and a launch is expected in 2015.

We suggest a number of items to pursue as future work. First, no effort has been made here to optimize the channel sets for best calibration algorithm performance. Channels with additional opacity should be considered. Second, algorithm sensitivity analyses could be performed with respect to antenna beamwidth, pointing accuracy/jitter, sensor noise, radiometer sample rate (angular spacing), and orbital characteristics. Third, the radiative transfer simulations can be improved by removing the constraint of spherical homogeneity. This could be done by considering multiple profiles along the line of sight, as is done in [25]. Fourth, the minimization routines could be executed using all channels instead of each channel individually. This could be accommodated, for example, by using 1DVAR minimization with *a priori* constraints on the gain and offset angle that are derived from prelaunch characterizations. Finally, we suggest the analysis of any microwave sounder data collected during a spacecraft maneuver that might be serendipitously colocated with operational GPSRO observations.

Acknowledgment

The authors gratefully acknowledge many helpful conversations with Prof. J. Martinez (Northeastern University) on the Microwave Radiometer Technology Acceleration antenna design, Prof. E. Miller (Tufts University) on limb data processing, and the Micro-sized Microwave Atmospheric Satellite team at the Massachusetts Institute of Technology Space Systems Laboratory. Opinions, interpretations, conclusions, and recommendations are those of the authors and are not necessarily endorsed by the United States Government.

REFERENCES

[1] M. A. Janssen, "An introduction to the passive microwave remote sensing of atmospheres," in *Atmospheric Remote Sensing by Microwave Radiometry*, M. A. Janssen, Ed. New York, NY, USA: Wiley, 1993, ch. 1.

[2] A. Wallard and W. Zhang, "Measurement Challenges for Global Observation Systems for Climate Change Monitoring: Traceability, Stability, and Uncertainty," WMO/TD-No. 1557: IOM-Rep. 105, 2010.

[3] D. Gu, D. Houtz, J. Randa, and D. K. Walker, "Extraction of illumination efficiency by solely radiometric measurements for improved brightness-temperature characterization of microwave blackbody target," *IEEE Trans. Geosci. Remote Sens.*, vol. 50, no. 11, pp. 4575–4583, Nov. 2012.

[4] W. Yang, H. Meng, R. R. Ferraro, I. Moradi, and C. Devaraj, "Cross-scan asymmetry of AMSU-A window channels: Characterization, correction, and verification," *IEEE Trans. Geosci. Remote Sens.*, vol. 51, no. 3, pp. 1514–1530, Mar. 2013.

[5] D. B. Kunkee, G. A. Poe, S. D. Swadley, Y. Hong, and M. Werner, "Special Sensor Microwave Imager Sounder (SSMIS) radiometric calibration anomalies part I: Identification and characterization," *IEEE Trans. Geosci. Remote Sens.*, vol. 46, no. 4, pp. 1017–1033, Apr. 2008.

[6] S.-P. Ho, W. Schreiner, and X. Zhou, "Using SI-traceable global positioning system radio occultation measurements for climate monitoring," *Bull. Amer. Meteor. Soc.*, vol. 91, no. 7, pp. S36–S37, 2009.

[7] L. Cucurull, "Improvement in the use of an operational constellation of GPS radio occultation receivers in weather forecasting," *Weather Forecast.*, vol. 25, no. 2, pp. 749–767, Apr. 2010.

[8] L. Cucurull, J. C. Derber, and R. J. Purser, "A bending angle forward operator for global positioning system radio occultation measurements," *J. Geophys. Res.*, vol. 118, no. 1, pp. 14–28, Jan. 2013.

[9] E. R. Kursinski, G. A. Hajj, J. T. Schofield, R. P. Linfield, and K. R. Hardy, "Observing Earth's atmosphere with radio occultation measurements using the Global Positioning System," *J. Geophys. Res.*, vol. 102, no. 1, pp. 23 429–23 465, Oct. 1997.

[10] C. O. Ao, G. A. Hajj, T. K. Meehan, D. Dong, B. A. Iijima, A. J. Mannucci, and E. R. Kursinski, "Rising and setting GPS occultations by use of open-loop tracking," *J. Geophys. Res.*, vol. 114, no. D4, pp. D04101-1–D04101-15, Feb. 2009.

[11] S. T. Brown, S. Desai, W. Lu, and A. B. Tanner, "On the long-term stability of microwave radiometers using noise diodes for calibration," *IEEE Trans. Geosci. Remote Sens.*, vol. 45, no. 7, pp. 1908–1920, May 2007.

[12] W. J. Blackwell, G. Allen, C. Galbraith, T. Hancock, R. Leslie, I. Osaretin, L. Retherford, M. Scarito, C. Semisch, M. Shields, M. Silver, D. Toher, K. Wight, D. Miller, K. Cahoy, and N. Erickson , "Nanosatellites for Earth environmental monitoring: The MicroMAS project," presented at the 26th Annual AIAA/USU Conf. Small Satellite, Logan, UT, USA, Aug. 2012, SSC12-XI-2.

[13] R. L. Bishop, D. A. Hinkley, D. R. Stoffel, D. E. Ping, P. R. Straus, and T. R. Brubaker, "First results from the GPS Compact Total Electron Content Sensor (CTECS) on the PSSC2 nanosat," presented at the 26th Annual AIAA/USU Conf. Small Satellite, Logan, UT, USA, Aug. 2012, SSC12-XI-2.

[14] W. Blackwell, L. Bickmeier, R. Leslie, M. Pieper, J. Samra, C. Surussavadee, and C. Upham, "Hyperspectral microwave atmospheric sounding," *IEEE Trans. Geosci. Remote Sens.*, vol. 49, no. 1, pp. 128–142, Jan. 2011.

[15] P. W. Rosenkranz, "Absorption of microwaves by atmospheric gases," in *Atmospheric Remote Sensing Microwave Radiometry*, M. A. Janssen, Ed. New York, NY, USA: Wiley, Jul. 1993, ch. 2.

[16] H. J. Liebe, "MPM: An atmospheric millimeter-wave propagation model," *Int. J. Infrared Millimeter Waves*, vol. 10, no. 6, pp. 631–650, Jun. 1989.

[17] H. J. Liebe, P. W. Rosenkranz, and G. A. Hufford, "Atmospheric 60-GHz oxygen spectrum: New laboratory measurements and line parameters," *J. Quant. Spectrosc. Radiative*, vol. 48, no. 5–6, pp. 629–643, Nov./Dec. 1992.

[18] S.-P. Ho, G. Kirchengast, S. Leroy, A. J. Mannucci, A. Steiner, D. Hunt, W. Schreiner, S. Sokolovskiy, C. Ao, M. Borsche, A. von Engeln, U. Foelsche, S. Heise, B. Iijima, Y.-H. Kuo, R. Kursinski, B. Pirscher, M. Ringer, C. Rocken, and T. Schmidt, "Estimating the uncertainty of using GPS radio occultation data for climate monitoring: Inter-comparison of CHAMP refractivity climate records 2002–2006 from different data centers," *J. Geophys. Res.*, vol. 114, no. D23, pp. 629–643, 2009.

[19] S.-P. Ho, M. Goldberg, Y.-H. Kuo, C.-Z. Zou, and W. Schreiner, "Calibration of temperature in the lower stratosphere from microwave measurements using COSMIC radio occultation data: Preliminary results," *Terr. Atmosp. Ocean. Sci.*, vol. 20, no. 1, pp. 87–100, 2009.

[20] S.-P. Ho, D. Hunt, A. K. Steiner, A. J. Mannucci, G. Kirchengast, H. Gleisner, S. Heise, A. von Engeln, C. Marquardt, S. Sokolovskiy, W. S. Schreiner, B. Scherllin-Pirscher, C. O. Ao, J. Wickert, S. Syndergaard, K. B. Lauritsen, S. Leroy, E. R. Kursinski, Y.-H. Kuo, U. Foelsche, T. Schmidt, and M. E. Gorbunov, "Reproducibility of GPS radio occultation data for climate monitoring: Profile-to-profile inter-comparison of CHAMP climate records 2002 to 2008 from six data centers," *J. Geophys. Res.*, vol. 117, no. D18111, 2012, doi:10.1029/2012JD017665.

[21] E. K. Smith and S. Weintraub, "The constants in the equation for atmospheric refractivity index at radio frequencies," *Proc. IRE*, vol. 41, no. 8, pp. 1035–1037, Aug. 1953.

[22] D. Thayer, "An improved equation for the radio refractive index of air," *Radio Sci.*, vol. 9, no. 10, pp. 803–807, Oct. 1974.

[23] J. A. Nelder and R. Mead, "A simplex method for function minimization," *Comput. J.*, vol. 7, no. 4, pp. 308–313, 1965.

[24] C. Muth, P. Lee, J. Shiue, and W. A. Webb, "Advanced Technology Microwave Sounder on NPOESS and NPP," in *Proc. IEEE IGARSS*, Sep. 2004, vol. 4, pp. 2454–2458.

[25] W. G. Read, Z. Shippony, and W. V. Snyder, "EOS MLS Forward Model Algorithm Theoretical Basis Document," Jet Propulsion Laboratory, Pasadena, CA, USA, 2003. [Online]. Available: http://mls.jpl.nasa.gov/data/eos_fwd_mdl_atbd.pdf

William J. Blackwell (S'92–M'02–SM'07) received the B.E.E. degree in electrical engineering from the Georgia Institute of Technology, Atlanta, GA, USA, in 1994 and the S.M. and Sc.D. degrees in electrical engineering and computer science from the Massachusetts Institute of Technology (MIT), Cambridge, MA, USA, in 1995 and 2002, respectively.

Since 2002, he has worked at the Lincoln Laboratory, MIT, Cambridge, where he is currently an Assistant Leader of the Sensor Technology and System Applications group. His primary research interests are in the area of atmospheric remote sensing, including the development and calibration of airborne and spaceborne microwave and hyperspectral infrared sensors, the retrieval of geophysical products from remote radiance measurements, and the application of electromagnetic, signal processing, and estimation theory. He serves on the NASA Atmospheric InfraRed Sounder (AIRS) and NPP science teams, the Joint Polar Satellite System Sounding Operational Algorithm Team, and the National Academy of Sciences Committee on Radio Frequencies. He is the Principal Investigator on the Micro-sized Microwave Atmospheric Satellite program, comprising a high-performance passive microwave spectrometer hosted on a 3U CubeSat planned for launch in 2014 and the Microwave Radiometer Technology Acceleration CubeSat planned for launch in 2016. He was previously the Integrated Program Office Sensor Scientist for the Advanced Technology Microwave Sounder on the Suomi National Polar Partnership launched in 2011 and the Atmospheric Algorithm Development Team Leader for the National Polar-Orbiting Environmental Satellite System (NPOESS) Microwave Imager/Sounder.

Dr. Blackwell held a National Science Foundation Graduate Research Fellowship from 1994 to 1997 and is a member of Tau Beta Pi, Eta Kappa Nu, Phi Kappa Phi, Sigma Xi, the American Meteorological Society, the American Geophysical Union, and Commission F of the International Union of Radio Science. He is currently an Associate Editor of the IEEE TRANSACTIONS ON GEOSCIENCE AND REMOTE SENSING and the IEEE GEOSCIENCE AND REMOTE SENSING (GRSS) MAGAZINE. He is the Chair of the IEEE GRSS Frequency Allocations for Remote Sensing technical committee, the IEEE GRSS Remote Sensing Instruments and Technologies for Small Satellites working group, and the Boston Section of the IEEE GRSS. He was the recipient of the 2009 NOAA David Johnson Award for his work in neural network retrievals and microwave calibration and is the coauthor of *Neural Networks in Atmospheric Remote Sensing* (Artech House, 2009). He received a poster award at the 12th Specialist Meeting on Microwave Radiometry and Remote Sensing of the Environment in March 2012 for "Design and Analysis of a Hyperspectral Microwave Receiver Subsystem" and was selected as a 2012 recipient of the IEEE Region 1 Managerial Excellence in an Engineering Organization Award "for outstanding leadership of the multi-disciplinary technical team developing innovative future microwave remote sensing systems."

Rebecca Bishop received the B.S. degree in physics and mathematics from the University of Idaho, Moscow, ID, USA, in 1996, and the M.S. and Ph.D. degrees in physics from the University of Texas at Dallas, Richardson, TX, USA, in 1997 and 2001, respectively.

From 2001 to 2004, she held a postdoctoral position with Clemson University, Clemson, SC, USA, and also received the National Science Foundation's CEDAR Postdoctoral Fellowship during that period. In 2004, she joined the Space Science Application Department, The Aerospace Corporation, El Segundo, CA, USA, where she continues to work as a Research Scientist.

Kerri Cahoy (S'00–M'08) received the B.S. degree in electrical engineering from Cornell University, Ithaca, NY, USA, in 2000, and the M.S. and Ph.D. degrees in electrical engineering from Stanford University, Stanford, CA, USA, in 2002 and 2008, respectively.

After working as a Senior Payload and Communication Sciences Engineer at Space Systems Loral, she completed a NASA Postdoctoral Program Fellowship at the NASA Ames Research Center and held a research staff appointment with the Massachusetts Institute of Technology (MIT)/NASA Goddard Space Flight Center. She is currently a Boeing Assistant Professor in the Department of Aeronautics and Astronautics, MIT, Cambridge, MA, USA with a joint appointment in the Department of Earth and Planetary Sciences at MIT, Cambridge.

Brian Cohen, photograph and biography not available at the time of publication.

Clayton Crail received the B.S. degree in aerospace engineering from The University of Texas at Austin, Austin, TX, USA, in 2007, and the S.M. degree in aeronautics and astronautics and the M.B.A. degree from the Massachusetts Institute of Technology (MIT), Cambridge, MA, USA, in 2013 as part of the Leaders for Global Operations Program.

In 2008, he joined Lincoln Laboratory, MIT, Lexington, MA, USA, where he is currently a member of the Technical Staff. His current research interests include space systems architecture analysis and design, small satellite technology, remote sensing, lean manufacturing, orbit analysis, and satellite communications.

Lidia Cucurull received the Ph.D. degree in physics from the Barcelona University, Barcelona, Spain, in 2001.

Since then, she has worked with the University Corporation for Atmospheric Research, Boulder, CO, USA, the National Aeronautics and Space Administration, Goddard Space Flight Center Greenbelt, MD USA, National Oceanic and Atmospheric Administration (NOAA), National Weather Service, Silver Spring, MD, and the NOAA National Environmental Satellite, Data and Information Services. She is currently the NOAA Chief Scientist for Satellite GPS Radio Occultation with the NOAA's Earth System Research Laboratory, Office of Oceanic and Atmospheric Research, Boulder, CO.

Dr. Cucurull has won several national awards in recognition of her work. She was the recipient of the 2007 UCAR Outstanding Scientific and Technology Advancement Award and the 2011 NOAA David Johnson Award.

Pratik Dave received the B.S. degree in aerospace engineering from the University of Maryland, College Park, MD, USA, in 2009. He is currently working toward the S.M. degree in aeronautics and astronautics at the Massachusetts Institute of Technology (MIT), Lexington, MA, USA, as a Lincoln Scholar.

He has since been working at the Lincoln Laboratory, MIT, Lexington, as an Assistant Research Staff in the area of space systems analysis.

Michael DiLiberto, photograph and biography not available at the time of publication.

Neal Erickson (M'78) received the B.S. degree from the California Institute of Technology, Pasadena, CA, USA, in 1970, and the Ph.D. degree from the University of California, Berkeley, CA, in 1979.

Since 1979, he has been with the Astronomy Department, University of Massachusetts Amherst, Amherst, MA, USA, where he is currently a Research Professor. He has been extensively involved in the field of low-noise millimeter- and submillimeter-wave receiver systems and astronomical observations with these systems. He has also designed the Schottky diode mixers and varactor frequency multipliers, quasi-optical systems, and low-noise HEMT amplifiers, and much of the receiver system for the Submillimeter Wave Astronomy Satellite. In 1982, he cofounded Millitech, Northampton, MA, USA, and in 2000, he founded Erickson Instruments LLC, Amherst, MA.

Chad Fish was born in Utah, UT, USA. He received the B.S. and M.S. degrees in electrical engineering from Utah State University, Logan, UT.

He has served as a Branch Lead, Research Scientist, Project Manager, Systems Engineer, and Electrical Engineer on various space station, small satellite, and sounding rocket projects. His technical background is in upper atmospheric radar and remote sensing techniques in situ and remote ionospheric sensing techniques, and high-speed analog and digital electronics. He was the Program Manager with the National Science Foundation-sponsored Dynamics Ionosphere CubeSat Experiment, which comprised of two identical orbit picosatellites to make high-resolution temporal and spatial measurements of ionospheric electric and magnetic fields and plasma density and temperature. He has also been the Program Manager with the National Aeronautics and Space Administration-sponsored Floating Potential Measurement Unit and the Solar Occultation for Ice Experiment on the Aeronomy of the Ice in the Mesosphere mission.

Shu-peng Ho received the B.S. degree in computer engineering from Feng Chia University, Taichung City, Taiwan, in 1987, the M.S. degree in meteorology from Rutgers, The State University of New Jersey, Piscataway, NJ, USA, in 1992, the M.S. degree in atmospheric science from the University of Wisconsin-Madison, Madison, WI, USA, in 1995, and the Ph.D. degree in atmospheric science from the University of Wisconsin-Madison, Madison, in 1998.

He has worked at Analytical Service and Materials, Inc., in affiliation of the NASA Langley Research Center, Hampton, VA, as a Research Scientist. Since 2001, he has worked at National Center for Atmospheric Research/University Corporation for Atmospheric Research, Boulder, CO, USA. His primary research interests are in the area of climate variability and change analysis using satellite remote sensing data. He serves on the NASA Tropospheric Emission Spectrometer science team, the World Climate Research Programme (WCRP) Global Energy and Water Cycle Experiment (GEWEX) science team, the WCRP Global Stratospheric Processes and their Role in Climate science team, the International Radio Occultation Working Group, and the International Radio Occultation (RO) Trend Working Group science team. He is also the Team Leader for the NOAA National Climatic Data Center Global Positioning System RO climate data record. He has published more than 37 journal papers in the related fields.

Dr. Ho was the recipient of the UCAR Outstanding Accomplishment Award for Scientific and Technical Advancement (for the Measurements of Pollution In The Troposphere project) in 2006, the Key Contributor to the UCAR COSMIC Program Award in 2006, and the recipient of the COSMIC Special Recognition Award for coordinating the COSMIC Student Program in 2008.

R. Vincent Leslie received the B.S. degree from Boston University, Boston, MA, USA, and the M.S. and Ph.D. degrees from Massachusetts Institute of Technology (MIT), Cambridge, MA, in 1998, 2000, and 2004, respectively, all in electrical engineering.

He was a Graduate Research Assistant with the Remote Sensing and Estimation Group, Research Laboratory of Electronics, MIT, specializing in passive microwave radiometry. He is a member of the Technical Staff in the Sensor Technology and System Applications Group.

Mr. Leslie is a member of the Order of the Engineer.

Adam B. Milstein received the B.S. and Ph.D. degrees in electrical engineering from Purdue University, Hammond, IN, USA, in 2000 and 2004, respectively.

In 2004, he joined Lincoln Laboratory, Massachusetts Institute of Technology, Lexington, MA, USA, as a member of the Technical Staff. Since 2011, he has contributed to validation and refinement of the stochastic cloud clearing/neural network retrieval algorithm used as the first guess for Atmospheric Infrared Sounder/Advanced Microwave Sounding Unit sounding products. Since 2007, he has also contributed to the GOES-R project, including verification of Advanced Baseline Imager Level 1b Image Navigation and Registration performance. His recent research interests include atmospheric sounding retrieval algorithms, modeling of optical scatter from aerosols, biomedical optics, and inverse imaging problems.

Idahosa A. Osaretin (S'07–M'11) received the B.S. degree in electrical and computer engineering, the M.S. degree in electrical engineering, and the Ph.D. degree in electrical engineering from the Ohio State University, Columbus OH, USA, in 2006, 2010, and 2011, respectively.

Since 2011, he has been with Lincoln Laboratory, MIT, Lexington, MA, USA, where he is currently a member of the Technical Staff. His current research interests include microwave radiometer design and analysis, compact reflector antenna design, low-profile ultrawideband antenna design and analysis, microwave circuits, and electromagnetic wave propagation (radiation, scattering, and wave guiding) in complex environments.